IEEE Access
Multidisciplinary | Rapid Review | Open Access Journal

Received 18 May 2022, accepted 13 June 2022, date of publication 22 June 2022, date of current version 25 July 2022.

Digital Object Identifier 10.1109/ACCESS.2022.3185241

On Design of a Triple Elliptical Super Wideband Antenna for 5G Applications

M. AYYAPPAN, (Graduate Student Member, IEEE), AND PRAGATI PATEL, (Senior Member, IEEE)

Department of Electronics and Communication Engineering, National Institute of Technology Goa, Farmagudi, Ponda, Goa 403041, India

Corresponding author: M. Ayyappan (ayyappan995@gmail.com)

This work was supported by the Science and Engineering Research Board (SERB), Department of Science and Technology (DST), Government of India, under Project ECR/2017/003341.

ABSTRACT A novel compact triple elliptical monopole antenna has been designed, analyzed and fabricated for super wideband applications. To enhance the impedance bandwidth, the author proposed a monopole antenna with a triple elliptical patch excited by a 50Ω triangular tapered microstrip feedline. Further improvement is achieved by optimally modifying the Defected Ground Structure (DGS) of the antenna. The proposed patch structure is mounted on a Roger's RT-Duroid 5880 substrate (ϵ_r= 2.2, tan δ = 0.0009) and has compact physical dimensions of 27 mm × 29.5 mm. The fabricated antenna covers the frequency band from 1.91 GHz to 43.5 GHz for $S_{11} \leq -10$ dB with a fractional bandwidth of > 183.17% and has a ratio bandwidth of 22.77:1. This extended bandwidth coverage permits the antenna to operate for wide range of application including 5G and Internet of Things (IoT). The proposed antenna has a very high Bandwidth Dimension Ratio (BDR) of 5761.87 which makes it the best candidate for superwideband antenna. Far field measurements disclose an omnidirectional radiation pattern across the frequency of operation. Further, the farfield Radar Cross Section (RCS) is analyzed through simulation and it is to be noted that relatively low values are obtained through out the frequency of operation. In addition, the compactness of the proposed antenna is theoretically verified with the aid of fundamental dimension limit theorem.

INDEX TERMS 5G mobile communication, bandwidth dimension ratio (BDR), fundamental dimension limit theorem, Internet of Things (IoT), monopole superwideband antenna, tapered feed.

I. INTRODUCTION

With the advent of various sophisticated technologies in the wireless communication domain, the telecommunication industry has grown at a rapid rate over the years. Amidst the increasing growth in network and data traffic, fifth generation (5G) communication systems has been deployed to comply with the above constraints [1]. Owing to this 5G wireless system can provide an extended frequency spectrum and increased data rates up to multi GigaBites per Second (Gbps). Apart from the already existing fourth generation (4G) band, some additional bands alloted for 5G communications are n78 (3.3-3.6 GHz) which is also known as sub-6 GHz band and it offers a higher data rate compared to the 4G LTE (Long Term Evolution) frequency band. Next one are the millimeter wave bands (26, 28, 40, 50 and 66 GHz) [2]. In addition 5G communication system has an important role to play in the domain of Internet of Things (IoT) as these devices require an increased data rate to operate on. This brings an increased demand for small sized antennas with an enhanced bandwidth enough to support IoT devices [3].

With the technological advancement, the demand for communication systems with higher data rates and spectral efficiency is escalating. The necessity for high data rate wireless communication over short distances can be met with Ultra Wide-Band (UWB) radio technology [4]. However, when a single antenna is used for various communication systems in a single portable device for long-range data transfers, they may be inconsequential. In this situation, a recent trend has been to use a super wideband antenna, which can provide ubiquitous coverage by covering both short and long range transmission [5].

Multidimensional research has been performed for different antenna configurations to incorporate the advantages

The associate editor coordinating the review of this manuscript and approving it for publication was Bilal Khawaja.

of Super Wide-Band (SWB) technology in modern wireless applications [5]. Many different bandwidth enhancement techniques, such as Defective Ground Structure (DGS) and fractal patch structures [6]–[10], [12], [13], as well as a broad range of feeding techniques, such as microstrip tapered feed line and Co-Planar Waveguide (CPW) feed, have been suggested by antenna designers in order to achieve wider bandwidth. In [6], a super-wideband propeller shaped printed monopole antenna is presented. The enhanced bandwidth is achieved by encompassing a propeller on the disc of a typical circular disc monopole with a CPW feed. This design has an impedance bandwidth ratio of 11.6:1, allowing it to cover a wide range of frequencies from 3 GHz to 35 GHz. The suggested antenna's gain ranges from 4 to 5.2 dBi. For super-wideband applications, a novel textile fractal antenna is developed and the patch is built using a consecutive iterations of triangle and circle and later optimized using a genetic algorithm in [7]. This monopole antenna generates an impedance bandwidth that covers the frequency range of 1.4 GHz to 20 GHz. This design uses a partially modified elliptical ground plane to achieve wider bandwidth and is mainly employed in the development of wireless body area networks. A compact circular fractal antenna element loaded with a central pentagonal slot and a compact super wideband microstrip monopole antenna in the shape of a human skull is proposed in [8] and [9] respectively. Reference [10] investigates a compact concentric structured monopole patch antenna is proposed for superwideband applications. Reference [11] proposes a planar compact SWB antenna that performs between 20 GHz and 120 GHz, covering mmWave and large Multiple Input Multiple Output (MIMO) applications for 5G. This antenna, on the other hand, has not been experimentally validated and performs poorly in the low-frequency 5G bands. Reference [12] shows yet another low-profile wideband MIMO antenna for 5G devices, albeit it is a band-specific antenna that does not meet the concept of SWB. A super wide bandwidth is obtained without any kind of dissipative loading using a Bowtie antenna in [13]. In spite of having a broader fractional bandwidth, the gain of these antennas are small and the main beam tends to tilt beyond a 4:1 bandwidth due to the defective ground structure. However these effects are reduced with the aid of parasitic loop as directors. Another technique to achieve superwideband characterisitcs is by tapering the ground plane and feedline [14]

In the future generation of wireless communication system, it is very much critical to make the devices compact. So under this scenario, the compactness of the antenna is verified with the aid of fundamental dimension limit theorem. The electrical size of the antenna calculated analytically is with in the Mclean and Chu fundamental limit curves after comparison of proposed antenna with Chu and Mclean's classical limitation theories. Therefore offers the largest possible bandwidth for the lowest feasible size [15].

The purpose of this antenna design is to ensure faster and more effective 5G communication, with the primary goals of reduced complexity, lower cost, increased bandwidth for future applications, and excellent resilience to attenuation and interference. UWB antennas have shorter wavelengths and wider bandwidths, allowing for faster data transmission. Organizations and research enterprises all over the world are working to integrate high-speed and high-efficiency antennas into communication networks. The successful use of these high-speed antennas will improve the effectiveness of wireless communication, allowing countries and organisations to engage more wirelessly. Integration of the presented antenna into communication networks can hone education enhancement technologies such as E-learning programmes due to its capacity to operate successfully in the lower sub-6 GHz and millimeter-wave bands. The proposed antenna offers super-wideband capability and also ensures higher data rate which leads to super fast internet. These metrics allow the antenna to support the integration of IoT and Fifth generation communication systems in devices. These effective integration with IoT devices will prepare the human kind to communicate better during pandemic situations such as COVID-19 [16].

In this proposed work, a tapered fed printed triple elliptical monopole antenna is designed and investigated. The design makes use of a triple elliptical radiator along with a tapered feed and DGS structure to enhance the wideband performance. This combination of the later generates a monopole structure. The design begins with a conventional elliptical radiator. To improve the bandwidth and matching, the above conventional elliptical antenna is modified by the adjoining the rotated copy of the ellipse to the either side of the conventional elliptical antenna. The proposed antenna is made from a nature inspired leaves and the structure reveals a nature inspired fractal. The novelty of the proposed antenna not only lies in the arrangement of the ellipses with respect to the tapered feed but also in the DGS design which helps in improving the bandwidth. The incorporation of the circular slot helps in extending the current path length without modifying the actual dimensions of the antenna. The main highlight of the proposed radiator is its higher Bandwidth Dimension Ratio (BDR) and bandwidth, which is achieved by enhancing the electrical length of the radiator. The proposed antenna has an extremely high BDR of 5761. In view of this, the proposed antenna structure attains wider bandwidth in the range of 1.91 GHz - 43.5 GHz with a %bandwidth of $> 183.17\%$. It is to be noted that such a wider bandwidth is achieved for a compact size of 27×29.5 mm^2. The overall size reduction of 75.58% is achieved with this design when compared with a conventional elliptical radiator with respect to the lower resonant frequency. Moreover, to analyze the compactness of the antenna, comparison of the designed antennas with Chu and Mclean's classical limitation theories shows that the mathematically computed antenna electrical is with in the Mclean and Chu fundamental limit curves [17], [18]. This infers that the proposed antenna has exceptional performance because of the maximum achievable bandwidth for the smallest possible size. The simulation

TABLE 1. Parameters and dimensions of the proposed antenna.

Parameters	Values(mm)	Parameters	Values (mm)
L_s	29.5	A_G	0.25
W_s	27	W_2	0.3
W_f	2.29	r_5	1
L_g	10.2	L_2	5
a_1	1.22	h_t	0.035
a_2	9.08	h	0.787
r_s	3	S	0.70
W_t	1.3	b	7.5
L_M	9	L_F	10.4

and antenna modelling are carried out in CST microwave studio.

II. ANTENNA CONFIGURATION

The configuration of the proposed antenna is illustrated in Figure 1 and the detailed dimensions are tabulated in TABLE 1. The dimensions of the proposed antenna are optimized through parametric analysis. The proposed design is mounted on a Roger's RT-Duroid 5880 dielectric material with a dielectric constant of $\epsilon_r = 2.2$, loss tangent of $\tan\delta = 0.0009$ and a thickness of 0.787 mm. It is to be noted that the proposed antenna consists of a triple integrated ellipses fed with a microstrip tapered feed line along with the novel DGS structure is responsible for the SWB characteristics of the antenna.

Figure 1 shows the schematic of the proposed antenna. The design is evolved from the basics of a monopole antenna. The antenna consists of three parts: the patch section, tapered feed region and DGS section. The tapered feedline alongside with the elliptical patch improves the antenna performance and matching and helps in resonance shifting for SWB operation. The tapered feedline concatenated with the main patch aids in smoothening the current path, resulting in a broader impedance bandwidth. Hence, this monopole antenna is fed by a tapered triangular feed line which is optimized to 50 Ω impedance matching to reduce incident wave reflection. The tapered feed line's width at the bottom end corresponds to a characteristic impedance of 50 Ω, and the width at the top end have a characteristic impedance of 75 Ω. It has been described that the use of symmetrical feed to a planar monopole antenna can support the excitation of the vertical characteristics mode and efficiently stimulate vertical current component on the radiating patch, leading to the enhancement in impedance bandwidth The tapered feed line, together with the monopole antennas tends to have enhanced bandwidth performance and can transmit UWB pulses with minimal distortion.

The dimensions of printed monopoles were calculated using the planar disc monopole antenna formulation [19], [20] and it is schematically represented in Figure 1. The lower frequency of the planar disc monopole antenna, which corresponds to VSWR = 2, is calculated with respect to,

$$f_L = \frac{c}{\lambda} = \frac{7.2}{L_M + r + S} \tag{1}$$

where L_M is the length of the equivalent monopole antenna,r is the effective radius of the equivalent cylindrical monopole antenna (which is equal to $\pi \times a \times b$) and S is the feed gap optimized to $S = 0.7$ mm. This configuration has a dielectric layer on one side of the printed monopole and this dielectric substrate enhances the monopole's effective dimensions, which inturn lowers the f_L. As a result, the more acceptable equation for f_L is as follows:

$$f_L = \frac{7.2}{(L_M + r + S)\,k} GHz \tag{2}$$

Here the value of k is 1.15 which is mathematically derived for a dielectric substrate with $\epsilon_r = 2.2$ and $h = 0.787$ mm. The effective radius of the cylindrical monopole antenna is given by:

$$r = \frac{T}{(2 \times \pi \times L_M)} \tag{3}$$

where T denotes the semi-elliptical monopole radiating patch's area. The bandwidth exhibits good matching over an ultra-broadband frequency range as a result of this curvature. W_t is iteratively calculated and does not depend on the resonant frequency in the triangular tapered feed line parameters whereas W_f is optimized for 50 Ω.

A. EVOLUTION OF THE PROPOSED ANTENNA

The design evolution begins with a conventional elliptical radiator as depicted in Figure 2 (a). The design provided a bandwidth of 68.5 GHz and has a percentage bandwidth of 185.68% with five stop bands and is shown in TABLE 2. As the evolution proceeds towards the second stage, a copy of the previous ellipse rotated at an angle of $\theta = 18.5°$ is concatenated with the elliptical radiator in Stage I and is illustrated in Figure 2 (b). For the next stage, the same process done in Stage II is carried out with an only difference of θ rotated at an angle of -18.5° resulting in the structure shown in Figure 2 (c). In Stage II and Stage III, the behavior of the proposed structure remains the same and provides a bandwidth of 186.56% with three notch bands as shown in Figure 3 and same is presented in TABLE 2. The structures in Stage II and Stage III are adjoined together to form the structure in Stage IV. As the design proceeds from Stage I to Stage IV, the electrical length of the antenna is significantly increased. Consequently, it improves the current path length which eventually increases the effective inductance and capacitance resulting in bandwidth enhancement. This henceforth improves the Bandwidth Dimension Ratio (BDR) of the proposed antenna. As a result, Stage IV has improved the bandwidth to 187.06% with a single stop band from 8.34 GHz - 10.08 GHz. Further, a circular slot is inscribed into stage IV so as to bring the notched bands to pass band thereby fulfilling the conditions of super wideband antennas which is illustrated in stage V in Figure 2 (e).

The variations of S_{11} vs Frequency for different stages are illustrated in Figure 3. Corresponding bandwidth and frequency ranges for each iteration are tabulated in TABLE 2.

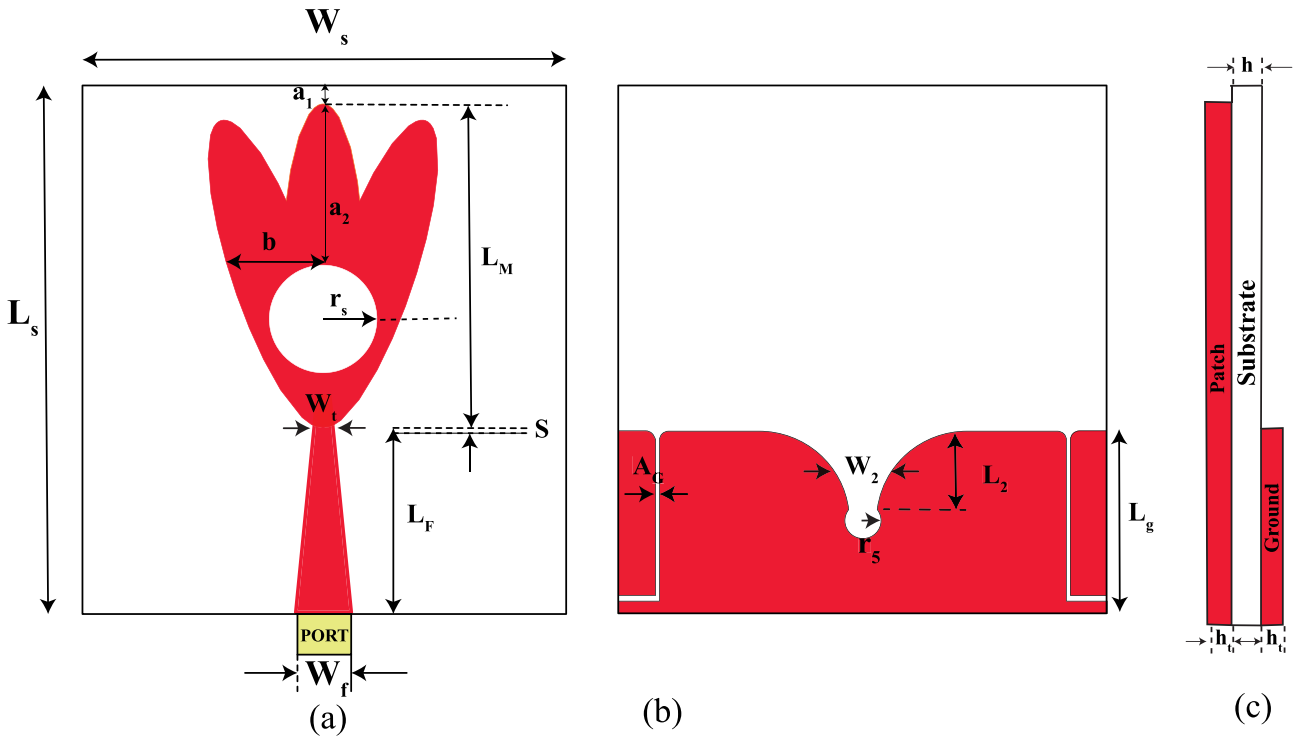

FIGURE 1. Schematic of the proposed antenna structure (a) Front view (b) Rear view (c) Side view.

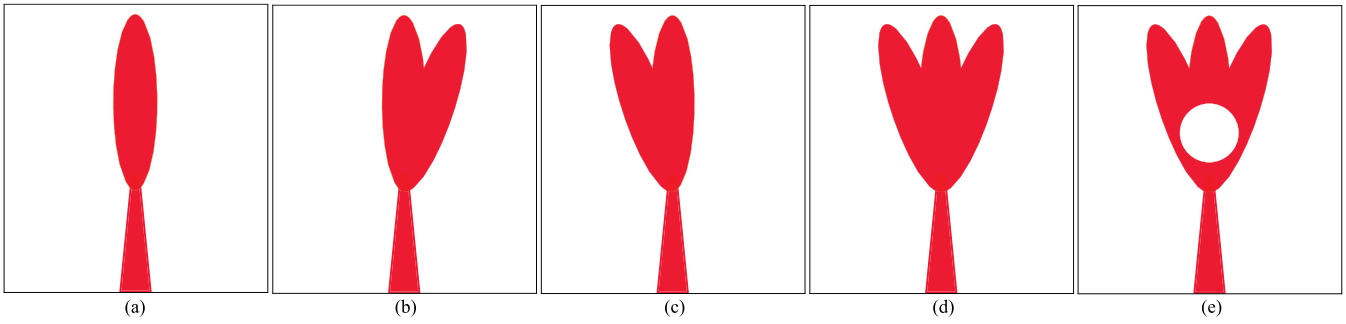

FIGURE 2. Evolution of the proposed antenna (a) Stage I, (b) Stage II, (c) Stage III, (d) Stage IV, (e) Stage V.

TABLE 2. Bandwidth comparison for each stages.

Stages	Bandwidth [GHz]	% Bandwidth	Notched Bands
I	68.5 (2.644-71.14 GHz)	185.68	4.68−6.78 GHz 8.22-10.44 GHz 13.62-15.9 GHz 18.96-20.22 GHz 23.04-24.28 GHz
II and III	68.34 (2.46-70.8 GHz)	186.56	8.90-10.12 GHz 14.52-15.75 GHz 32.39-33.02 GHz
IV	68.57 (2.37-70.94 GHz)	187.06	8.34-10.08 GHz
V	69.25 (2.11-71.36 GHz)	188.51	-

III. FUNDAMENTAL LIMITATION THEORY FOR COMPACT ANTENNAS

Generally electrically small size antennas or compact antennas are expressed with reference to it's radian length, $l = \frac{\lambda}{2\pi}$ and the largest dimension of the antenna, a. Considering the wavenumber as $k = \frac{2\pi}{\lambda}$, an electrically compact antenna is expected to have the following inequality:

$$a \leq \frac{\lambda}{2\pi} \leq \frac{1}{k}$$
$$ka \leq 1$$

Quality Factor (Q) being one of the key antenna parameter demonstrates an inequality between the antenna's electrical size and bandwidth. Hence Q is mathematically expressed as:

$$Q = \begin{cases} \dfrac{2\omega W_{Ee}}{P_{radiated}} & W_{Ee} \geq W_{Me} \\ \dfrac{2\omega W_{Me}}{P_{radiated}} & W_{Me} \geq W_{Ee} \end{cases} \quad (4)$$

The time-average, non-propagating, stored electric and magnetic energy is represented by W_{Ee} and W_{Me}, respectively. ω

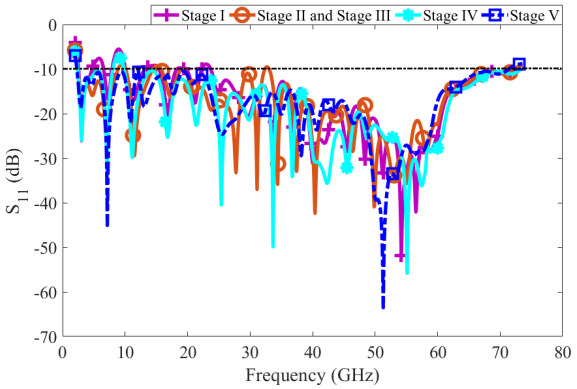

FIGURE 3. Simulated S_{11} vs Frequency plot for different iteration stages for the proposed antenna.

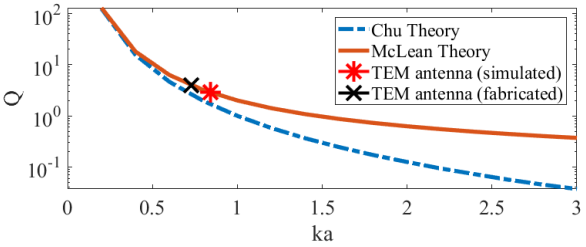

FIGURE 4. Comparitive analysis of proposed SWB antennas (simulated and fabricated) with the Chu and McLean curves.

denotes the angular frequency. $P_{radiated}$ represents the power that has been radiated. The Q is speculated as the reciprocal of its bandwidth at higher values and is shown in eqn. (5). Lower the values of Q, on contrary, causes the antenna input impedance to vary slowly with frequency, resulting in a broad bandwidth capacity of the antenna [21].

$$Bandwidth = \frac{f_{upper} - f_{lower}}{f_{center}} = \frac{1}{Q} \tag{5}$$

L.J. Chu developed the following expression of Q for the lowest Transverse Magnetic (TM) mode [17]:

$$Q = \frac{1 + 3k^2a^2}{k^3a^3[1 + k^2a^2]} \tag{6}$$

This is in contrast to the result of his equivalent second-order network, which is given as:

$$Q = \frac{1 + 2k^2a^2}{k^3a^3[1 + k^2a^2]} \tag{7}$$

As $ka \ll 1$, the equation is modified as below:

$$Q \cong \frac{1}{k^3a^3} \tag{8}$$

This eqn. implies that reducing the antenna size leads to a considerable increase in Q. As a result, comparing Eq. no. (5) and (8) demonstrates that reducing antenna size effectively reduces bandwidth. As a result, having an optimally improved bandwidth while reducing size is a major problem for electrically smaller antennas.

McLean developed a new methodology to compute the antenna's Q. This technique, in contrast to Chu's methodology, provides an accurate equation for Q calculation. McLean's equation agrees with Chu's equation for higher values of Q whereas the two hypotheses disagree as lower values of Q [18].

Mclean's Equations for calculating Q is shown below:

$$Q = \frac{1}{k^3a^3} + \frac{1}{ka} \tag{9}$$

It is necessary to apply fundamental limit theory to the existing antennas and compare it with the practical antennas in order to verify its effectiveness. In the literature, such a technique has been used on a variety of antennas, with the conclusion that none of them exceed the fundamental limitation theory. As a result, Chu and McLean's classic theories are seen to provide realistic boundaries [22].

IV. EVALUATION OF PROPOSED ANTENNA'S ELECTRICAL SIZE

The antenna electrical size is calculated for the corresponding patch height to evaluate the antenna performance with respect to size and bandwidth. The fractional bandwidth of the antenna is improved whereas the antenna's electrical size is decreased due to improved antenna volumetric efficiency. Typically, traditional antennas don't make optimal use of their spherical volumes due to which is not close as possible to the Chu and McLean curves' fundamental dimension. The most effective utilization of enclosed spaces are by minimizing the non-radiated stored energy of the antenna, hence increasing its impedance bandwidth. The wavelength that corresponds to an antenna's working frequency (λ) aids in determining its size or dimensions. Normally, when evaluating the antenna size of a narrowband antenna, the wavelength for the center frequency (λ_c) is taken into account, however this is not the case for UWB/SWB antennas. The traditional fundamental limitation theories are based on the wavenumber for the antenna's lower operating frequency ($k = \frac{2\pi}{\lambda}$). As a result, these ideas are best applied to the design of narrowband antennas because the wavelength difference between the center and edge frequencies is much smaller in these designs. However, the wavelength corresponding to the center frequency significantly varies across the wavelength corresponding to the lower and upper frequencies is analyzed during the detailed examination of the wavelengths of the UWB/SWB antenna for different frequency of operation. As a result, the concept of using the wavelength corresponding to the center frequency directly for the entire range of frequencies is not feasible for UWB/SWB antennas. Instead, defining the antenna's electrical size to satisfy the equation $k_La \leq 1$ is a more acceptable technique. The wavenumber corresponding to the lower bound of occupied bandwidth is denoted by k_L. For the entire designed and fabricated prototype, Table 3 shows the product (k_La) for the wavenumber (k_L) and the antenna sphere radius *(a)*.

TABLE 3. Electrical size calculation of the proposed antenna.

Approach	Patch Height (mm)	f_L (GHz)	Wavelength at λ_L	Wavenumber (k_L)	$k_L a$ (rad)
Simulated	0.035	2.21	135.74	0.0463	0.84
Measured	0.035	1.91	157.06	0.0400	0.73

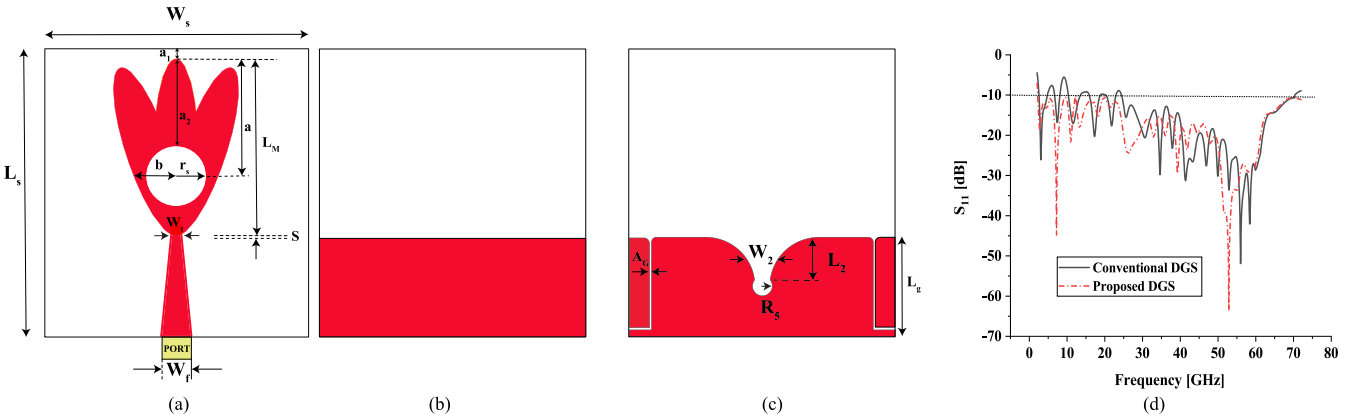

FIGURE 5. Layout of the proposed antenna (a) Front view (b) Conventional DGS (c) Proposed DGS (d) S_{11} response of the proposed antenna with conventional DGS and proposed DGS.

The quality factor Q of the simulated and fabricated antenna is plotted again *ka* is shown in Figure 4 which evaluates the comparative analysis of proposed SWB antennas (simulated and fabricated) with the Chu and McLean curves. The proposed antenna's quality factor is analyzed using McLean's equation, and it is to be noted that the proposed antenna agrees well with the McLean's curve of the fundamental dimension limit theorem. Hence it can be asserted that the proposed super wideband antenna is designed close to the fundamental dimension limit theorem [15].

V. PARAMETRIC STUDY OF THE PROPOSED ANTENNA

In this section, each parameter of the proposed antenna is optimized by varying one parameter and keeping the other parameters fixed. For the proposed structure, parametric analysis is performed for the DGS. DGS is mainly employed to vary the surface current distribution of the antenna. This perturbations indeed results in the variation of inductance and capacitance of the feed line. The introduction of rectangular defect in the ground plane, not only increases the effective inductance but also increase the fringing electric field and thereby increasing parasitic capacitance. This parasitic capacitance enhances the coupling between the ground and feed resulting in the improvement of bandwidth.In order to start the parametric analysis of the DGS, the proposed antenna with conventional DGS and optimized DGS is shown in Figure 5 (b) and Figure 5 (c) respectively.

The S_{11} response with conventional DGS is shown in Figure 5 (d). It can be observed that the S_{11} curve has multiple notched bands over the frequency range of operation. To obtain superwideband characteristics it is critical enough to convert this notched bands in to pass band. Hence the parametric analysis begins with the DGS structure. The parametric values of slot1 (first rectangular slot) with dimension $L_2 \times W_2$ are optimized in such a way to enhance the bandwidth. The position of the slot has been optimized for getting the wider bandwidth and better impedance matching by iterating through various positions and assorted distance from the center of the patch. The values of L_2 are varied from 4 mm to 6 mm. It is to be noted that the impedance bandwidth is better at 3 mm when compared to 1 mm and 3 mm. With the optimization of L_2, the notched band at 7.2 GHz has been modified to a passband. Further, the width of the slot is modified by varying it from 2 mm to 4 mm. The slot width was affecting the current distribution at 13 GHz. Variation of slot width has widened the current distribution at 13 GHz resulting in the conversion of notched band in to pass band at 13 GHz, but still a small portion is above -10 dB. To bring that band further below -10 dB, next a circular slot with radius R_5 is etched at the base of the first rectangular slot as shown in Figure 6 (c). However still a notched band exists at 19 GHz. In order to widen the current distribution further, an air gap A_G is introduced in to the DGS, and the parameter is varied from 0.15 mm to 0.35 mm in steps of 0.10 mm. This air gap has excited the band at 19 GHz, with which the superwideband characteristics is achieved as shown in Figure 6 (d).

VI. RESULTS AND DISCUSSION

This section analyzes the experimental and simulated results. The proposed design illustrated in Figure 1 is analyzed and simulated in CST microwave studio 2019 using Finite Integration Technique (FIT). The proposed miniaturized antenna

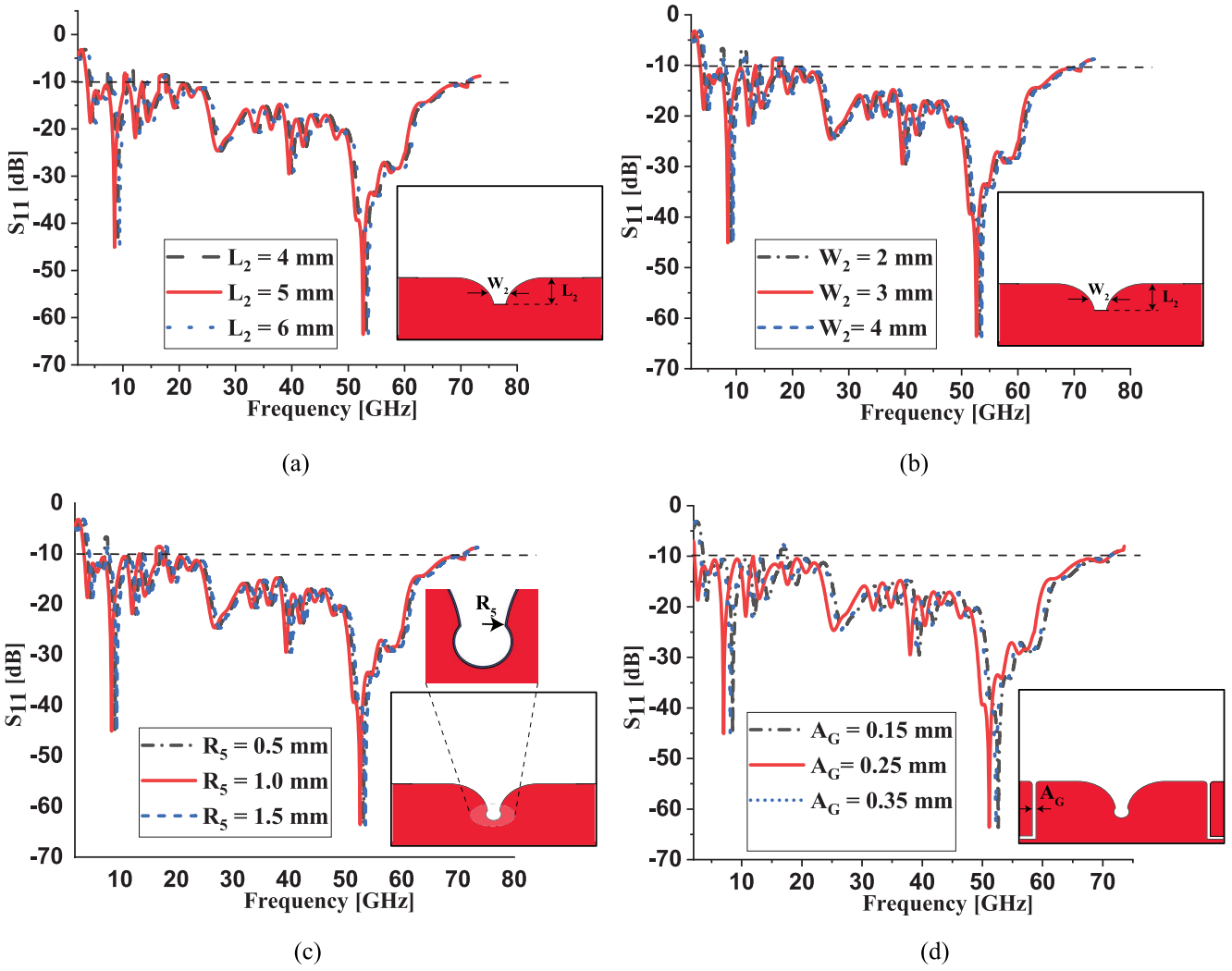

FIGURE 6. Variation of S_{11} vs Frequency for different parameters (a) L_2 (b) W_2 (c) r_5 (d) A_G.

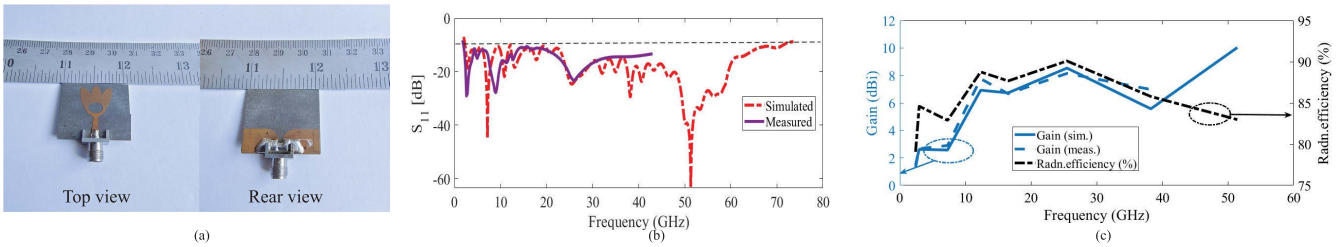

FIGURE 7. (a) Fabricated prototype of the proposed antenna (b) Measured and Simulated Reflection coefficient and (c) Measured and Simulated Gain and Simulated Radiation Efficiency vs Frequency plots.

is manufactured through the LPKF PCB prototyping machine and the measurements are performed with the aid of Keysight PNA Vector Network Analyzer (10 MHz - 43.5 GHz) in order to validate the simulation results. Figure 7 (a) showcases the fabricated prototype of the proposed antenna. The simulated and measured reflection coefficient for S_{11} $\leq$-10 dB are plotted in Figure 7 (b). Fractional bandwidth of more than 183.17% [1.91 GHz - 43.5 GHz] and 188.51% [2.11 GHz - 71.36 GHz] is achieved during measurement and fabrication respectively. It is to be noted that the range of VNA used for measurement is till 43.5 GHz. Measured result shows good agreement with simulated results, and slight variation in result might be due to fabrication inconsistencies.

A. GAIN AND RADIATION EFFICIENCY

The simulated and measured broadside gain of the triple elliptical antenna is depicted in Figure 7 (c). It reveals that the realized gain tends to increase with frequency and maintains

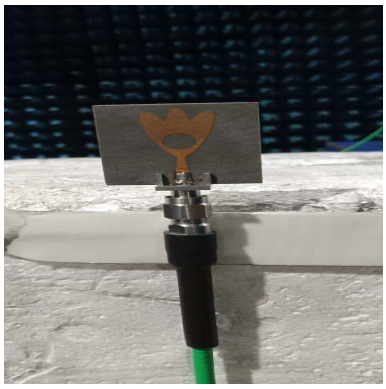

FIGURE 8. Radiation pattern measurement setup in anechoic chamber.

a positive gain throughout the frequency of operation. This is due to, the effective aperture of the radiating patch at higher frequencies is larger than the wavelength corresponding to that f_H. Reason behind the above hypothesis is that the antenna gain is directly proportional to the antenna's effective aperture and wavelength.

The gain of the antenna might get attenuated at higher frequencies due to the connector losses. The measured peak gain has a minimal gain of 1.51 dBi at 2.40 GHz and maximum of 8.15 dBi at 27.97 GHz and shows good agreement with the simulated results. These gain values are in good accord with the gains of similar antennas reported in the existing literatures. It is observed from Figure 7 (c) that the radiation efficiency increases with the increase in frequency. Peak efficiency of 90.08% is achieved at 27.97 GHz. After 27.97 GHz, there is a gradual reduction in the radiation efficiency due to the impedance mismatching at higher frequencies due to the SMA connector.

B. RADIATION PATTERN AND CURRENT DISTRIBUTION

Radiation pattern being an important parameter measures the power focusing capability of the antenna in a particular direction. Figure 8 shows the measurement setup for radiation pattern along with the device under test. Figure 9 (a) to Figure 9 (f) shows the measured and simulated e-plane and h-plane radiation patterns for frequencies at 3.10 GHz, 10.82 GHz, and 27.97 GHz respectively. Far-field azimuth ($\theta = 90°$) and elevation ($\phi = 90°$) radiation patterns are analyzed for radiation pattern measurement for the above three frequencies. The measured findings reveal that the suggested antenna has a stable radiation pattern and cross polarization values over -20 db over the entire operating frequency range. The multipath effect is also reduced considering the low cross polarization levels. Current distributions at different frequencies are illustrated in Figure 10 (a) - (d). Due to the presence of substantially higher quantity of current in the feed line thus creates an insight in to the mode variation. The first-order harmonic resonance (fundamental mode) is observed at the lowest operational frequency i.e. 3.10 GHz under close examination. From Fig. 10 (a), it is evident that

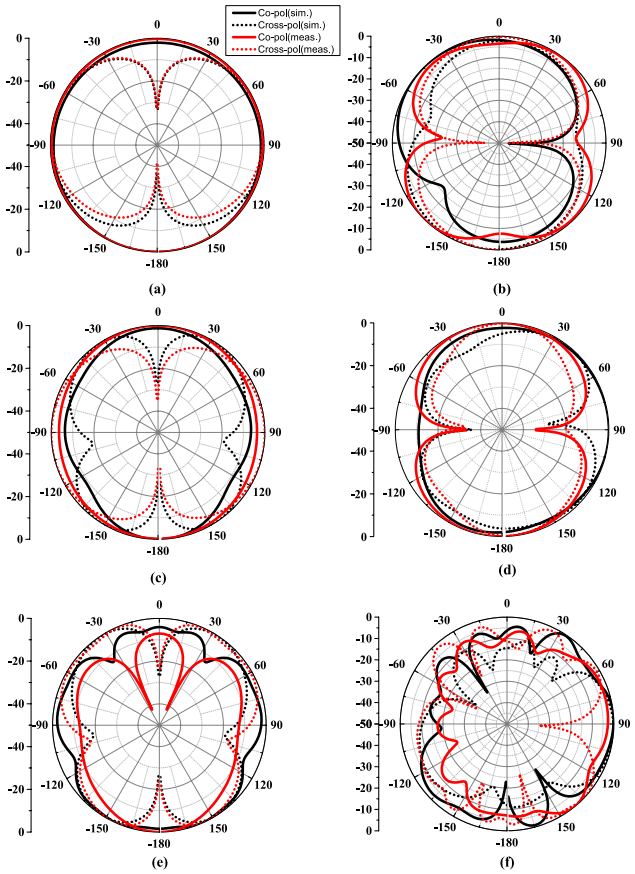

FIGURE 9. 2-D measured and simulated radiation pattern (a) e-plane at 3.10 GHz (b) h-plane at 3.10 GHz (c) e-plane at 10.82 GHz (d) h-plane at 10.82 GHz (e) e-plane at 27.97 GHz (f) h-plane at 27.97 GHz.

the current propagate along the feedline and lower half of the elliptical radiator. As shown in Figure 10 (a), this results in a standing wave with a significant envelope bump. The circular slots are also surrounded by the standing waves, generating a current null around them. Hence, the radiation pattern in Figure 9 (a) is shaped like a donut with zero emission from the antenna's top side.

The radiated power is primarily restricted to the front side of the antenna due to the accumulation of current along the bottom side of the elliptical radiator. The higher-order modes emerge as the frequency rises, as inferred from the current distribution at 10.82 GHz. The second-order harmonic are detected at this very frequency and the current distribution is mainly concentrated near the lower portion of the radiating patch. Moreover, current also propagate around the top angular portions of the radiating triple ellipse as shown in Figure 10 (b). Due to this propagation, a standing wave forms around the top of the radiator's perturbing slots. The antenna top suffers a radiating null as a result of this standing wave, similar to the case of first resonant frequency at 3.10 GHz. Under this scenario, antenna's far-field pattern still exhibit a donut structure with most of the radiated power is accumulated around the antenna's front

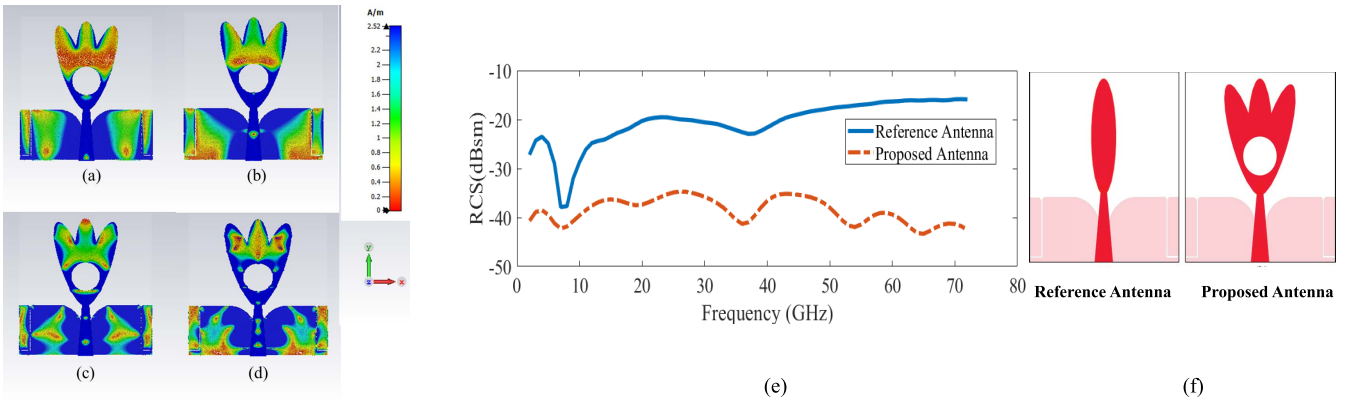

FIGURE 10. Current distribution at (a) 3.10 GHz (b) 10.82 GHz (c) 15.60 GHz (d) 27.97 GHz and (e) Simulated RCS value over the frequency range of operation (f) Reference antenna and proposed antenna used for RCS analysis.

side and around the top side of the elliptical radiator. From Figure 10 (c), it is revealed that there are more resonating modes, and the current distribution on the antenna surface forms a butterfly-shaped standing wave. Here the radiating nulls appears around the portions of antenna correlating to the vertices's of the butterfly shaped standing wave. Because of the current being distributed around the standing wave, the antenna radiates primarily towards directions of the surface current. This standing wave dominates the antenna's emission over lower frequency ranges such as 3.10 GHz, 10.82 GHz and 15.60 GHz, as shown in the previous studies [32].

Moreover, with the increase in frequency, the higher order harmonics also increases which inturn results in to a complex distribution along the antenna structure. As a result of this distribution, the triple elliptical patch operates in a hybrid mode, comprising both standing and traveling waves. In this scenario, the traveling wave is the most critical factor. However, a standing wave is generated around the circular slots and the elliptical radiator, as seen in Figure 10 (d). As a result, the current largely travels through a variety of distributed places on the edges of the elliptical radiator, causing a significant amount of current null on the radiator surface. As illustrated in Figure 9, this provides an insight into the deteriorated radiation pattern at 27.97 GHz. In addition, the radiated power gets suppressed in the front and rear side of the patch. These radiating patch edges provides the major contribution to form the far-field radiation, resulting in a deviated omnidirectional pattern as shown in Figure 9 (e) and Figure 9 (f) [32].

C. RADAR CROSS SECTION ANALYSIS

The proposed design is very much compatible for military reasons due to its compact size and wide operational bandwidth. The antenna RCS is also investigated, despite the fact that achieving a low RCS value is not the primary goal of this research. Figure 10 (e) shows the far-field monostatic RCS calculations for both the reference and proposed antennas for a cross-polarized incident wave infringing from the antenna's normal direction. When the reference and proposed antennas

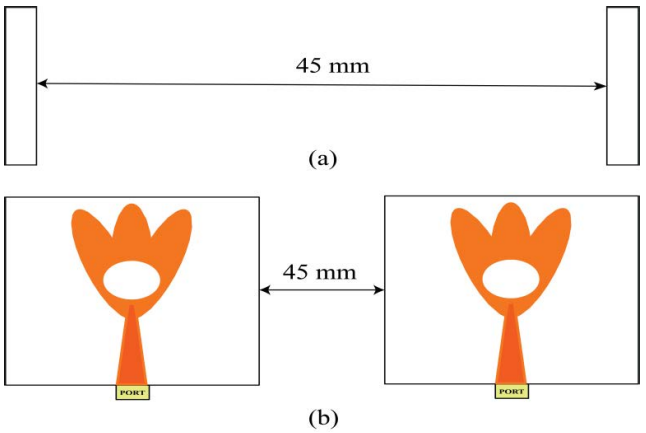

FIGURE 11. Time domain analysis setup for different configurations (a) Face to face (b) Side by side.

are compared, the proposed antenna has a significantly lower RCS. Furthermore, as illustrated in Figure 10 (e), the proposed antenna's RCS value varies between -42.15 and -37.26 dBsm depending on the frequency of operation. Here the RCS analysis is performed under the theta polarized incident angle ($\theta = 0°$ and $\phi = 0°$). Our main idea was to provide an insight in to the capability of the proposed work to be used for RADAR and military applications. The reference antenna and proposed antenna using in the RCS evaluation is illustrated in Figure 10 (f).

D. BANDWIDTH DIMENSION RATIO

BDR is an important super wideband antenna characteristic that depicts the relationship between the antenna's compactness and bandwidth. "BDR" denotes how much bandwidth a given antenna can deliver per unit of electrical area. BDR is defined mathematically as:

$$BDR = \frac{bandwidth\%}{\lambda_{length} \times \lambda_{width}} \tag{10}$$

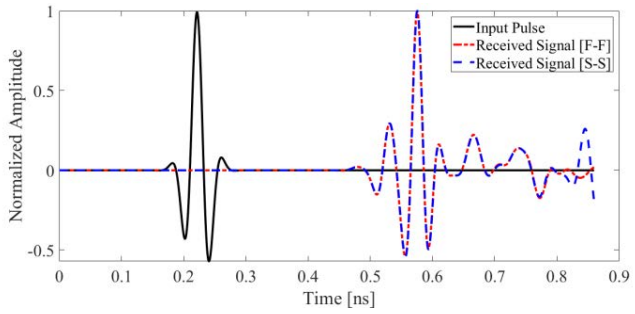

FIGURE 12. Simulated normalized amplitude of input and received pulses.

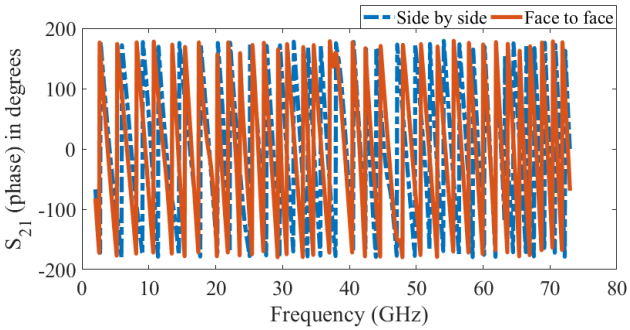

FIGURE 13. Phase variation in Side by side and Face to face configuration.

where, λ_{length} and λ_{width} are electrical length and width of the radiator, respectively, and "λ" is calculated with respect to the f_L. From eqn. (10), it can be seen that the proposed antenna's BDR is 5761, which is much higher compared to other antennas in the literature. Table 4 tabulates the comparison of proposed antenna's to the antennas of available literature. When compared to existing literatures, the suggested antenna has a high BDR when compared to all the literaures except the designs in [10], [37], [38]. These increase in BDR in [10], [37], [38] is due to the lower operating frequency achieved. However, the proposed antenna is compact when measured in terms of mm^2. It is understood that increase in the overall dimension of the antenna shifts the lower resonant frequency towards the left side. But the bandwidths are significantly higher than all the other designs. It is to be noted that the proposed antenna had a limited measurement facility of VNA which supports only upto 43.5 GHz.

VII. TIME DOMAIN ANALYSIS

The time domain analysis is basically employed to analyze the antenna's pulse shaping properties. The pulse duration is in the range of around 100 pico-seconds. In ideal case, the shape of the received SWB pulse should match with the shape of the transmitted pulse. However, due to the ringing effect, the received pulse tends to get skewed in shape and are prompt to have long tail. Under this scenario, the antenna should be designed properly to avoid such distortions thereby making the time domain analysis very much critical for wideband antennas. In order to perform the time domain characterization, two similar antenna configurations are aligned at a distance of 45 mm in each case. The two time domain analysis configuration setups (a) "Face to face" (b) "Side by side" are illustrated in Figure 11. Gaussian pulses are used for transmission and reception in both configurations as shown in Figure 12. A significant time domain parameter; Fidelity Factor (FF) which determines the equivalence between the transmitted and received pulses. A slight ringing is observed in both received pulses before the excitation occurs. This is due to the channel noise effect. However, both received pulses had the same pulse shape, indicating the transmitted data was received without loss.

The normalized transmission and reception pulses are provided in the following equations below.

$$\breve{T_s}(t) = \frac{T_s(t)}{[\int_{-\alpha}^{\alpha} |T_s(t)|^2 dt]^{1/2}} \tag{11}$$

$$\breve{R_s}(t) = \frac{R_s(t)}{[\int_{-\alpha}^{\alpha} |R_s(t)|^2 dt]^{1/2}} \tag{12}$$

The fidelity factor is given by

$$FF = max \int_{-\alpha}^{\alpha} \breve{T_s}(t)\breve{R_s}(t+\tau)dt \tag{13}$$

where, $\breve{T_s}(t)$ is the transmitted pulse, while the received pulse is $\breve{R_s}(t)$. After normalization, the value of FF is between 0 and 1. The signal pulse received is identical to the transmitted pulse without any system loss when the value of FF is 1. Similarly, a score of 0 indicates system attenuation, which means signal received is entirely mismatched from the transmitted signal. The received pulse, on the other hand, is utterly undetected at FF values below 0.5. As a result, high FF values guarantee that the signal received is distortion-free. Hence, closer the value of FF towards 1 minimizes the distortion in the received pulse. To calculate the fidelity factor, the input Gaussian pulse obtained in the Figure 12 is used to calculate the $\breve{R_s}(t)$, similarly the received pulses for both side by side and face to face configuration obtained from Figure 12 is used to calculate the $\breve{R_s}(t)$. Then both this $\breve{T_s}(t)$ and $\breve{R_s}(t)$ are cross-correlated as shown in eqn. (13) to calculate the fidelity factor for both the configurations using matlab The fidelity factor obtained for both side by side and face to face are 0.891 and 0.874 respectively. This ensures that received pulses are 89.1% and 87.4% similar to the transmitted pulse for side by side and face to face configurations respectively. From Figure 13, it is evident that the phase fluctuation in both the configurations are linear for the entire range of frequency, indicating that the pulse being received is free of out of phase components [10].

A. GROUP DELAY

Another important time domain characteristic is group delay and it is calculated theoretically as the negative derivative of phase change with respect to frequency. The signal undergoes amplitude and phase distortion as it passes through a device.

TABLE 4. Comparison of proposed antenna with previously reported antennas in literature.

Ref.	Dimension [λ^2]	OFR [GHz]	% BW	RBW	BDR	Peak Gain [dBi]
[6]	$0.38\lambda \times 0.55\lambda$	3-35	168.42	11.67:1	805.84	5.2 at 18 GHz
[7]	$0.28\lambda \times 0.285\lambda$	1.4-20	173.80	14.2:1	2178	-
[8]	$0.32\lambda \times 0.276\lambda$	3.45 - 52.17	175	14.9:1	1981.43	-
[9]	$0.20\lambda \times 0.24\lambda$	3 - 24	155.55	8:1	3240.6	6.78
[10]	$0.16\lambda \times 0.18\lambda$	1.25 - 40	188	32:1	6523	9.7
[13]	$0.32\lambda \times 0.32\lambda$	0.42-5.5	171.62	13:1	1676	7.96
[23]	$0.17\lambda \times 0.13\lambda$	0.96-10.9	167.22	11.35:1	**6975.2**	-
[24]	$0.30\lambda \times 0.23\lambda$	3.68-31.61	158	8.58:1	2289	9.78
[25]	$1.28\lambda \times 4.9\lambda$	24-40	68	-	3429.26	**19 at 34 GHz**
[26]	$0.27\lambda \times 0.32\lambda$	2.88-14	131.75	4.86:1	1424.88	7.8 at 12.39 GHz
[27]	$0.43\lambda \times 0.481\lambda$	4.37-16	114	3.66:1	551.77	2
[33]	$1.148\lambda \times 1.148\lambda$	17.22-180	165	10.45:1	125.2	10 at 110 GHz
[34]	$0.34\lambda \times 0.32\lambda$	3.4-37.4	166.67	11:1	1531.90	5.9 at 18 GHz
[35]	$0.47\lambda \times 0.31\lambda$	3.15-32	164.15	10.16:1	1102.9	-3.2 at 3 GHz
[36]	$0.30\lambda \times 0.29\lambda$	4.6-52	167.49	11.30:1	1903.20	4 (Average gain)
[37]	$0.16\lambda \times 0.13\lambda$	0.96 - 13.98	174.29	14.56:1	7468.51	5.5
[38]	$0.17\lambda \times 0.13\lambda$	0.95 - 13.8	173.96	14.58:1	7871	5.5
[39]	$0.42\lambda \times 0.5\lambda$	3 - 10.6	111.7	3.53:1	531.90	5.2
[40]	$0.29\lambda \times 0.265\lambda$	3.1 - 10.6	111.5	3.52:1	1450.87	7
[41]	$0.21\lambda \times 0.18\lambda$	2.74 - 13	130.7	4.74:1	3457.67	-
[42]	$0.326\lambda \times 0.28\lambda$	2.8 - 40	173.8	14.28:1	1904	7.16
[43]	$0.32\lambda \times 0.40\lambda$	1.2 - 15	170.3	12.5:1	1330.46	7
[44]	$0.239\lambda \times 0.239\lambda$	2.75 - 28	164	10:1	2871	4.80
Prop. (meas.)	$\mathbf{0.17\lambda \times 0.187\lambda}$	**1.91-43.5**	**183.17**	**10:1**	**2871**	**8.15 at 27.97 GHz**

Ref- References, OFR- Operating Frequency Range, BW - Bandwidth, RBW - Ratio Bandwidth, BDR- Bandwidth Dimension Ratio, Prop- Proposed

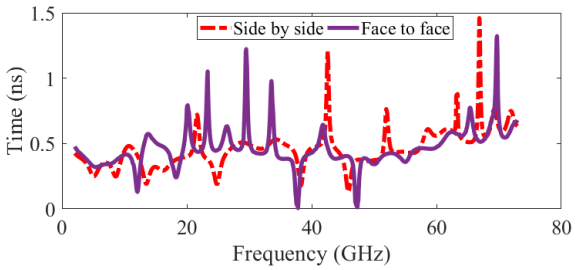

FIGURE 14. Group delay vs Frequency plot.

A wave that reaches a device's input has multiple frequency components. As a result, the group delay determines the average time delay of the input signal at each frequency. It also gives an indication of how dispersive the device is. The linear phase response for the entire far-field region is also validated by group delay. The group delay in a good SWB system should be as minimal as possible. The group delay should be constant or vary by less than 2 ns in practice, indicating a linear phase across the entire frequency range of operation. The actual amount of distortion in the transmitted pulse is determined by the linear phase response. The group delay can be calculated using eq.no 14.

$$\tau_g(\omega) = \frac{-d\varphi(\omega)}{d\omega} = \frac{d\varphi(\omega)}{2\pi\, df} \tag{14}$$

In this work, Figure 14 reveals that the group delay is well within the limits for both side by side and face to face configurations which makes it suitable for wireless communications [32].

VIII. RELEVANCE IN 5G

One of the critical attribute of the fifth generation communication system is the enhanced Mobile Broadband (eMBB). The deployment of eMBB will allow the 5G network to provide higher data rates, capacity, and coverage than previous generations. eMBB is essentially a more advanced form of 4G broadband [28]. The adoption of a unified and more sophisticated radio interface known as 5G New Radio (NR) ensures the progress of mobile broadband. The 5G NR worldwide standard has specified various frequency ranges in the mmWave bands in addition to the existing frequency spectrum of 4G LTE (26, 28, 40, 59, and 66 GHz) [29]. In order to deliver a ubiquitous connectivity for a broad range of applications, adaptive bandwidth technology with high spectrum flexibility has been employed [30]. As a corollary,

depending on the deployment, the 5G communication system will need to provide exceptionally high bandwidth ranging from below 1 GHz to 100 GHz. This creates a demand for low-cost, compact antennas that can cover a wide range of frequencies. The antenna presented in this paper covers the whole high-frequency spectrum of the 5G NR global standard while maintaining good gain and radiation efficiency. By supporting high traffic growth and expanding need for high-bandwidth connection, 5G radio technology becomes a crucial IoT enabler due to increased spectrum availability. The Internet of Things serves as a link between technological capabilities and business applications. 5G's widespread coverage, low latency, and high-speed connectivity enable a large number of IoT devices to communicate with one another in real time. As a result, a wide range of industrial applications will soon be able to benefit from such ground-breaking technology. In this regard, the suggested SWB antenna is an excellent contender because of its small size and ability to operate in the mmWave frequencies [31], [32].

IX. CONCLUSION

A novel triple elliptical monopole antenna is designed and analyzed for superwideband applications. Parametric analysis have been performed to optimize the parameters to enhance the impedance bandwidth of the antenna. With the aid of novel DGS structure and tapered feed, the bandwidth of the antenna is significantly enhanced. The proposed antenna has a BDR of 5761.87 which is high when compared to the existing literature. The proposed antenna provides an impedance bandwidth of more than 183.17% [1.91 GHz - 43.5 GHz] and 188.51% [2.11 GHz - 71.36 GHz] is achieved during measurement and fabrication respectively. The surface current analysis of the SWB antenna is used to theoretically explain the antenna's far-field behaviour at various frequencies. Moreover the compactness of the proposed antenna is mathematically verified using fundamental dimension limit theorem. Hence the proposed antenna finds application in S, C, X, Ka, Ku, Q band wireless communication systems and millimeter wave applications. In addition, the proposed SWB antenna is capable of covering the majority of current and future 5G application bands, including massive MIMO and mmWave. In light of the foregoing, it can be concluded that the developed antenna is a valuable addition to the antenna research community, as the high BDR SWB antenna offers operability in a variety of fascinating applications involving 5G, and IoT.

REFERENCES

[1] T. Rappaport, Y. Xing, G. R. MacCartney, A. F. Molisch, E. Mellios, and J. Zhang, "Overview of millimeter wave communications for fifth-generation (5G) wireless networks-with a focus on propagation models," *IEEE Trans. Antennas Propag.*, vol. 65, no. 12, pp. 6213–6230, Dec. 2017.

[2] G. Ancans, V. Bobrovs, A. Ancans, and D. Kalibatiene, "Spectrum considerations for 5G mobile communication systems," *Proc. Comput. Sci.*, vol. 104, pp. 509–516, Jan. 2017.

[3] S. Li, L. D. Xu, and S. Zhao, "5G Internet of Things: A survey," *J. Ind. Inf. Integr.*, vol. 10, pp. 1–9, Jun. 2018.

[4] J. Volakis, C.-C. Chen, and K. Fujimoto, *Small Antennas: Miniaturization Techniques and Applications*. New York, NY, USA: McGraw-Hill, 2009.

[5] W. Balani, M. Sarvagya, T. Ali, M. Pai M. M., J. Anguera, A. Andujar, and S. Das, "Design techniques of super-wideband antenna–existing and future prospective," *IEEE Access*, vol. 7, pp. 141241–141257, 2019.

[6] A. Gorai, A. Karmakar, M. Pal, and R. Ghatak, "A CPW-fed propeller shaped monopole antenna with super wideband characteristics," *Prog. Electromagn. Res.*, vol. 45, pp. 125–135, 2013.

[7] M. Karimyian-Mohammadabadi, M. A. Dorostkar, F. Shokuohi, M. Shanbeh, and A. Torkan, "Super-wideband textile fractal antenna for wireless body area networks," *J. Electromagn. Waves Appl.*, vol. 29, no. 13, pp. 1728–1740, 2015.

[8] D. Lodhi and S. Singhal, "Pentagon inscribed circular superwideband fractal MIMO antenna," *Int. J. Commun. Syst.*, vol. 35, no. 3, Feb. 2022, Art. no. e5039.

[9] M. A. Rahman, M. S. J. Singh, M. Samsuzzaman, and M. T. Islam, "A compact skull-shaped defected ground super wideband microstrip monopole antenna for short-distance wireless communication," *Int. J. Commun. Syst.*, vol. 33, no. 14, Sep. 2020, Art. no. e4527.

[10] W. Balani, M. Sarvagya, A. Samasgikar, T. Ali, and P. Kumar, "Design and analysis of super wideband antenna for microwave applications," *Sensors*, vol. 21, no. 2, p. 477, Jan. 2021.

[11] M. Alibakhshikenari, B. S. Virdee, C. H. See, R. A. Abd-Alhameed, F. Falcone, and E. Limiti, "Super-wide impedance bandwidth planar antenna for microwave and millimeter-wave applications," *Sensors*, vol. 19, no. 10, p. 2306, May 2019.

[12] D. Q. Liu, H. J. Luo, M. Zhang, H. L. Wen, B. Wang, and J. Wang, "An extremely low-profile wideband MIMO antenna for 5G smartphones," *IEEE Trans. Antennas Propag.*, vol. 67, no. 9, pp. 5772–5780, Sep. 2019.

[13] K. K. Ajith and A. Bhattacharya, "A novel compact superwideband bowtie antenna for 420 MHz to 5.5 GHz operation," *IEEE Trans. Antennas Propag.*, vol. 66, no. 8, pp. 3830–3836, Aug. 2018.

[14] S. Agrawal, Z. Wani, and M. S. Parihar, "Rectangular patch loaded circular monopole super wideband antenna with triple-band notch characteristic," *IETE Tech. Rev.*, pp. 1–12, Sep. 2021.

[15] S. Dey and N. C. Karmakar, "Design of novel super wide band antenna close to the fundamental dimension limit theory," *Sci. Rep.*, vol. 10, no. 1, pp. 1–15, Dec. 2020.

[16] O. Joseph, A. Silas, S. E. Donmaaye, T. J. Nawunzuk, V. Y. K. Loung, and N. T. Duah, "Design of a compact monopole antenna for super wideband and 5G applications," in *Proc. IEEE 8th Int. Conf. Adapt. Sci. Technol. (ICAST)*, Nov. 2021, pp. 1–5.

[17] L. J. Chu, "Physical limitations of omni-directional antennas," *J. Appl. Phys.*, vol. 19, no. 12, pp. 1163–1175, 1948.

[18] J. S. McLean, "A re-examination of the fundamental limits on the radiation Q of electrically small antennas," *IEEE Trans. Antennas Propag.*, vol. 44, no. 5, p. 672, May 1996.

[19] T. Yang, S.-Y. Suh, R. Nealy, W. A. Davis, and W. L. Stutzman, "Compact antennas for UWB applications," *IEEE Aerosp. Electron. Syst. Mag.*, vol. 19, no. 5, pp. 16–20, May 2004.

[20] J. Anguera, C. Puente, C. Borja, and J. Soler, "Fractal shaped antennas: A review," *Encyclopedia RF Microw. Eng.*, 2005.

[21] R. F. Harrington, "Effect of antenna size on gain, bandwidth, and efficiency," *J. Res. Nat. Bur. Standards, Sect. D, Radio Propag.*, vol. 64D, no. 1, p. 1, Jan. 1960.

[22] M.-C. Huynh, "Wideband compact antennas for wireless communication applications," Ph.D. dissertation, Dept. Elect. Comput. Eng., Virginia Tech, 2004.

[23] P. Okas, A. Sharma, G. Das, and R. K. Gangwar, "Elliptical slot loaded partially segmented circular monopole antenna for super wideband application," *AEU-Int. J. Electron. Commun.*, vol. 88, pp. 63–69, May 2018.

[24] S. Singhal, "Octagonal Sierpinski band-notched super-wideband antenna with defected ground structure and symmetrical feeding," *J. Comput. Electron.*, vol. 17, no. 3, pp. 1071–1081, 2018.

[25] P. Ramanujam, C. Arumugam, R. Venkatesan, and M. Ponnusamy, "Design of compact patch antenna with enhanced gain and bandwidth for 5G mm-wave applications," *IET Microw., Antennas Propag.*, vol. 14, no. 12, pp. 1455–1461, Oct. 2020.

[26] K. Neeshu and A. K. Tiwary, "Metamaterial loaded antenna with improved efficiency and gain for wideband application," *IETE J. Res.*, pp. 1–8, Dec. 2020.

[27] S. Kohar, S. Singh, and A. De, "Design of low profile cylindrical conformed microstrip patch antenna for wideband operation," *IETE J. Res.*, pp. 1–10, Jul. 2021.
[28] O. Teyeb, G. Wikstrom, M. Stattin, T. Cheng, S. Faxer, and H. Do, "Evolving LTE to fit the 5G future," *Ericsson Technol. Rev.*, vol. 95, no. 2, pp. 8–22, 2017.
[29] G. Ancans, V. Bobrovs, A. Ancans, and D. Kalibatiene, "Spectrum considerations for 5G mobile communication systems," *Proc. Comput. Sci.*, vol. 104, pp. 509–516, Jan. 2017.
[30] E. Dahlman, G. Mildh, S. Parkvall, J. Peisa, J. Sachs, and Y. Sköld, "5G radio access," *Ericsson Rev.*, vol. 6, no. 1, pp. 1–12, Jun. 2014.
[31] L. J. Young, "Telecom experts plot a path to 5G [news]," *IEEE Spectr.*, vol. 52, no. 10, pp. 14–15, Oct. 2015.
[32] S. Dey, M. S. Arefin, and N. C. Karmakar, "Design and experimental analysis of a novel compact and flexible super wide band antenna for 5G," *IEEE Access*, vol. 9, pp. 46698–46708, 2021.
[33] S. Singhal and A. K. Singh, "Asymmetrically CPW-fed circle inscribed hexagonal super wideband fractal antenna," *Microw. Opt. Technol. Lett.*, vol. 58, no. 12, pp. 2794–2799, 2016.
[34] S. Singhal and A. K. Singh, "CPW-fed hexagonal Sierpinski super wideband fractal antenna," *IET Microw., Antennas Propag.*, vol. 10, no. 15, pp. 1701–1707, Dec. 2016.
[35] S. Hakimi, S. K. A. Rahim, M. Abedian, S. M. Noghabaei, and M. Khalily, "CPW-fed transparent antenna for extended ultrawideband applications," *IEEE Antennas Wireless Propag. Lett.*, vol. 13, pp. 1251–1254, 2014.
[36] S. Singhal and A. K. Singh, "Modified star-star fractal (MSSF) super-wideband antenna," *Microw. Opt. Technol. Lett.*, vol. 59, no. 3, pp. 624–630, Mar. 2017.
[37] P. Okas, A. Sharma, and R. K. Gangwar, "Circular base loaded modified rectangular monopole radiator for super wideband application," *Microw. Opt. Technol. Lett.*, vol. 59, no. 10, pp. 2421–2428, 2017.
[38] P. Okas, A. Sharma, and R. K. Gangwar, "Super-wideband CPW fed modified square monopole antenna with stabilized radiation characteristics," *Microw. Opt. Technol. Lett.*, vol. 60, no. 3, pp. 568–575, 2018.
[39] H. A. E. Mohamed, A. S. Elkorany, S. A. Saad, and D. A. Saleeb, "New simple flower shaped reconfigurable band-notched UWB antenna using single varactor diode," *Prog. Electromagn. Res. C*, vol. 76, pp. 197–206, 2017.
[40] M. Rahanandeh, A. S. N. Amin, M. Hosseinzadeh, P. Rezai, and M. S. Rostami, "A compact elliptical slot antenna for covering Bluetooth/WiMAX/WLAN/ITU," *IEEE Antennas Wireless Propag. Lett.*, vol. 11, pp. 857–860, 2012.
[41] J. D. N. Cruz, R. C. S. Freire, A. J. R. Serres, L. C. M. D. Moura, A. P. D. Costa, and P. H. D. F. Silva, "Parametric study of printed monopole antenna bioinspired on the Inga marginata leaves for UWB applications," *J. Microw., Optoelectron. Electromagn. Appl.*, vol. 16, no. 1, pp. 312–322, Mar. 2017.
[42] S. Kundu and A. Chatterjee, "A compact super wideband antenna with stable and improved radiation using super wideband frequency selective surface," *AEU Int. J. Electron. Commun.*, vol. 150, Jun. 2022, Art. no. 154200.
[43] S. Agrawal, Z. Wani, and M. S. Parihar, "Patch loaded slot antenna for super wideband applications with dual-band notch characteristic," *Wireless Pers. Commun.*, vol. 123, no. 4, pp. 3051–3064, Apr. 2022.
[44] T. Tewary, S. Maity, S. Mukherjee, A. Roy, P. P. Sarkar, and S. Bhunia, "High gain miniaturrized super-wideband microstrip patch antenna," *Int. J. Commun. Syst.*, vol. 35, no. 11, Jul. 2022, Art. no. e5181.

M. AYYAPPAN (Graduate Student Member, IEEE) received the Bachelor of Technology (B.Tech.) degree in electronics and communication engineering and the Master of Technology (M.Tech.) degree in VLSI and embedded systems from the Cochin University of Science and Technology, Kerala, India, in 2014 and 2016, respectively. He is currently pursuing the Ph.D. degree in electronics and communication engineering with the National Institute of Technology Goa, Goa, India.

His research interests include superwideband antennas, multiple-input multiple-output antennas, and dielectric resonator antennas.

PRAGATI PATEL (Senior Member, IEEE) received the B.Tech. degree from the Dr. K. N. Modi Institute of Engineering and Technology, Modinagar, Ghaziabad, India, the M.Tech. degree from the Ambedkar Institute of Advanced Communication Technologies and Research (formerly Ambedkar Institute of Technology), Delhi, and the Ph.D. degree from the Indian Institute of Technology Bombay, Mumbai, India.

In 2016, she joined the Department of Electronics and Communication Engineering, National Institute of Technology Goa, Goa, India, as an Assistant Professor. She has authored or coauthored over 40 research articles in international peer-reviewed journals and conferences. Her research interests include microwave engineering, such as dielectric resonator antenna (DRA), microstrip patch antennas, and wireless power transmission. Her current research interests include dielectric resonators, antennas, and MIC. Her research interests include wireless power transmission, microstrip patch antennas, and dielectric resonator antennas for wireless communications. She has received the MHRD Fellowship during her Ph.D. degree and also the Early Career Fellowship from the Department of Science and Technology, Government of India, for pursuing research in the field of DRA. She was a recipient of the Young Scientist Award at URSI AT-RASC 2015. She actively involved in IEEE activities as a Secretary for educational activities of IEEE Bombay Section.